

Structure Analysis of Fe-Co and Fe-Co-B Alloy Thin Films Formed on MgO(001) Substrate

Kana Serizawa¹, Mitsuru Ohtake^{1,2}, Masaaki Futamoto¹, Fumiyoshi Kirino³, and Nobuyuki Inaba⁴

¹Faculty of Science and Engineering, Chuo University, 1-13-27 Kasuga, Bunkyo-ku, Tokyo 112-8551, Japan

²Faculty of Engineering, Kogakuin University, 2655-1 Nakano, Hachioji, Tokyo 192-0015, Japan

³Graduate School of Fine Arts, Tokyo University of the Arts, 12-8 Ueno-Koen, Taito-ku, Tokyo 110-8714, Japan

⁴Faculty of Engineering, Yamagata University, 4-3-16 Jyonan, Yonezawa, Yamagata 992-8510, Japan

Fe-Co and Fe-Co-B alloy films of 40 nm thickness are prepared by sputtering on MgO(001) single-crystal substrates using alloy targets of $(\text{Fe}_{0.7}\text{Co}_{0.3})_{100-x}\text{B}_x$ ($x = 0, 5, 10, 15$ at. %) by varying the substrate temperature from room temperature (RT) to 600 °C. The film structure is investigated by reflection high-energy electron diffraction and out-of-plane, in-plane, and pole-figure X-ray diffractions. Preparation condition of epitaxial film is found to depend on the B content and the substrate temperature. Epitaxial $(\text{Fe}_{0.7}\text{Co}_{0.3})_{100-x}\text{B}_x$ films are obtained at the investigated temperatures for the B contents lower than 5 at. %, whereas films with the B contents of 10 and 15 at. % grow epitaxially at temperatures higher than 400 and 600 °C, respectively. Single-crystal films of bcc(001) orientation are formed at temperatures higher than RT, 200, 400, and 600 °C for the B contents of 0, 5, 10, and 15 at. %, respectively. As the substrate temperature decreases, the epitaxial films with B contents of 5–15 at. % tend to involve four types of bcc(122) variant whose orientations are rotated around the film normal by 90° each other. The $(\text{Fe}_{0.7}\text{Co}_{0.3})_{90}\text{B}_{10}$ film deposited at RT and the $(\text{Fe}_{0.7}\text{Co}_{0.3})_{85}\text{B}_{15}$ films deposited at temperatures from RT to 200 °C are found to be consisting of bcc polycrystal and amorphous, respectively. The structure is thus determined to vary in the order of bcc(001) single-crystal => bcc(001) and bcc(122) epitaxial crystals => bcc polycrystal => amorphous with increasing the B content and with decreasing the substrate temperature. The lattices of single-crystal Fe-Co ($x = 0$ at. %) and Fe-Co-B ($x = 5$ –15 at. %) films are respectively expanded along the in-plane and the perpendicular directions. The single-crystal Fe-Co films show in-plane magnetic anisotropies with the easy magnetization directions of bcc[100] and bcc[010], which is reflecting the magnetocrystalline anisotropy of bulk bcc-Fe₇₀Co₃₀ alloy. On the contrary, the single-crystal Fe-Co-B films show almost isotropic in-plane magnetic properties and weak perpendicular anisotropies, which is possibly caused by an influence of lattice deformation along the perpendicular direction.

Key words: Fe-Co alloy, Fe-Co-B alloy, thin film, epitaxial growth, MgO single-crystal substrate, lattice strain, magnetic anisotropy

1. Introduction

Magnetic tunnel junctions consisting of tunnel barrier and ferromagnetic electrode layers have been studied for applications to tunnel magnetoresistance (TMR) sensors and magnetoresistive random access memory devices. In order to achieve high TMR ratios, highly-oriented polycrystalline¹⁾ or epitaxial single-crystal²⁾ MgO layer of (001) orientation is useful as the barrier layer.

Fe-Co and Fe-Co-B alloys with bcc structure are typical soft magnetic materials with high saturation magnetizations and have been frequently used as the electrode material. However, the crystallographic structure of Fe-Co-B film is affected by the B content^{3,4)} and the formation condition like annealing temperature^{5–8)}. Fe-Co-B film with a higher B content deposited at a lower substrate temperature tends to involve amorphous. The magnetic properties are also delicately influenced by the structure. Furthermore, it has been reported that perpendicular magnetic anisotropy is induced in Fe-Co and Fe-Co-B alloy films

when the crystal lattice is strained along the perpendicular direction^{9–16)}.

In order to investigate the basic structural and magnetic properties, it is useful to employ epitaxial films, since the crystallographic orientation can be controlled by the substrate orientation. However, there are few reports on the preparation of Fe-Co-B films on single-crystal substrates by systematically varying the formation condition. In the present study, $(\text{Fe}_{0.7}\text{Co}_{0.3})_{100-x}\text{B}_x$ films are prepared on MgO(001) substrates. The influences of B content and substrate temperature on the structure and the magnetic properties are investigated.

2. Experimental Procedure

A radio-frequency (RF) magnetron sputtering system equipped with a reflection high-energy electron diffraction (RHEED) facility was used for film formation. The base pressures were lower than 4×10^{-7} Pa. Polished MgO(001) substrates were heated at 600 °C for 1 hour to obtain clean surfaces. $(\text{Fe}_{0.7}\text{Co}_{0.3})_{100-x}\text{B}_x$ ($x =$

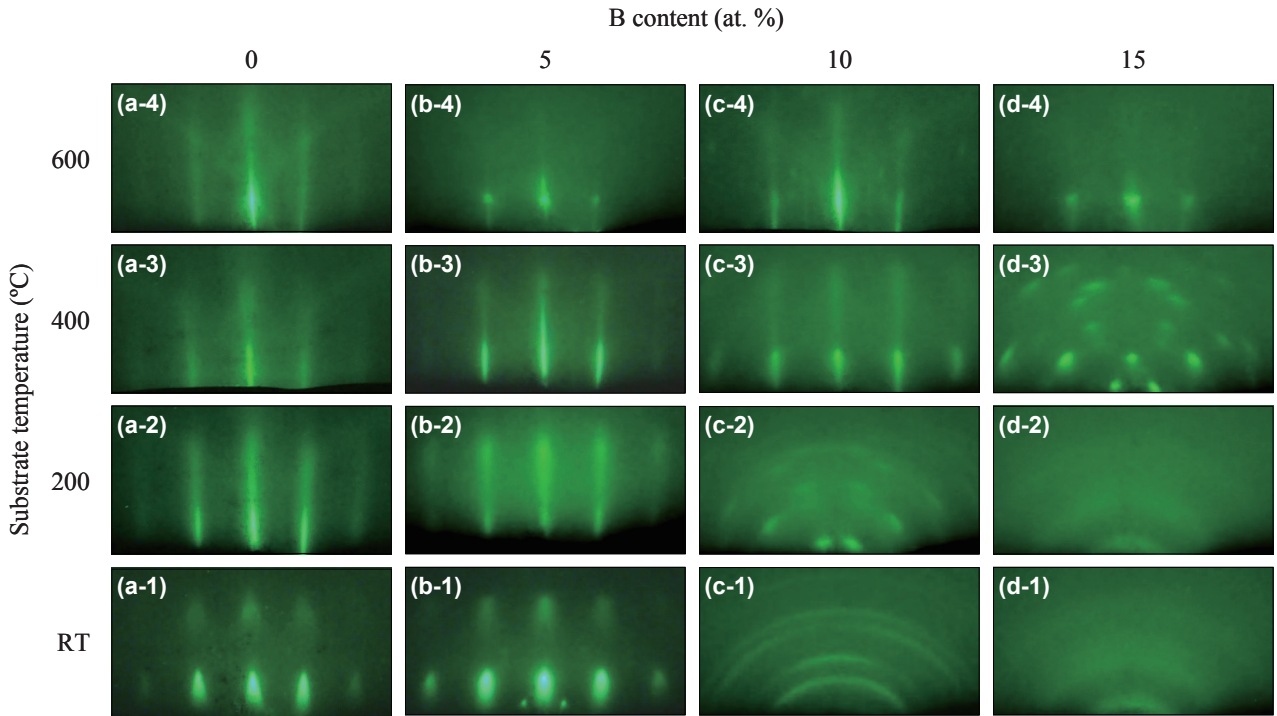


Fig. 1 RHEED patterns observed for $(\text{Fe}_{0.7}\text{Co}_{0.3})_{100-x}\text{B}_x$ films with the B contents of (a) 0, (b) 5, (c) 10, and (d) 15 at. % deposited on MgO(001) substrates at (a-1)–(d-1) RT, (a-2)–(d-2) 200 °C, (a-3)–(d-3) 400 °C, and (a-4)–(d-4) 600 °C. The incident electron beam is parallel to MgO[100].

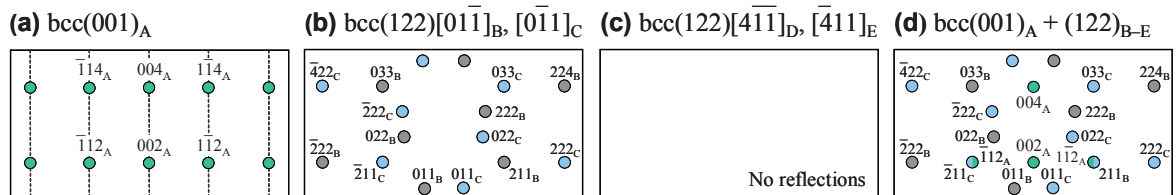


Fig. 2 Schematic diagrams of RHEED patterns simulated for (a) $\text{bcc}(001)$ and [(b), (c)] $\text{bcc}(122)$ surfaces. Schematic diagram of (d) is drawn by overlapping (a) and (b). The incident electron beam is parallel to (a) $\text{bcc}(001)[110]$, (b) $\text{bcc}(122)[01\bar{1}]$ and $[0\bar{1}1]$, or (c) $\text{bcc}(122)[4\bar{1}\bar{1}]$ and $[\bar{4}11]$.

0–15 at. %) alloy targets of 3 inch diameter were employed. The distance between target and substrate was fixed at 150 mm. The Ar gas pressure was kept constant at 0.67 Pa. The RF powers for alloy targets with the B contents of 0, 5, 10, and 15 at. % were respectively adjusted at 57, 65, 60, and 58 W, where the deposition rates were 0.02 nm/s. $(\text{Fe}_{0.7}\text{Co}_{0.3})_{100-x}\text{B}_x$ films of 40 nm thickness were deposited on the substrates at temperatures ranging from RT to 600 °C. In the present study, the film compositions were considered to be similar to the target compositions.

The surface structure was studied by RHEED. The structural properties were investigated by $2\theta/\omega$ scan out-of-plane, $2\theta/\chi/\phi$ scan in-plane, and pole-figure X-ray diffractions (XRDs) with Cu-K α radiation ($\lambda = 0.15418$ nm). The surface morphology was observed by atomic force microscopy (AFM). The magnetization curves were measured at RT by vibrating sample magnetometry.

3. Results and Discussion

3.1 Crystal structure and orientation

Figure 1(a) shows the RHEED patterns of $\text{Fe}_{70}\text{Co}_{30}$ ($x = 0$) films deposited on MgO(001) substrates at different temperatures observed by making the incident electron beam parallel to MgO[100]. Diffraction patterns corresponding to $\text{bcc}(001)$ single-crystal surface are recognized, as shown in the simulated pattern of Fig. 2(a). The epitaxial orientation relationship is determined as

$$\text{bcc}(\text{Fe}_{0.7}\text{Co}_{0.3})_{100-x}\text{B}_x(001)[110] \parallel \text{MgO}(001)[100].$$

(type A)

The $\text{Fe}_{70}\text{Co}_{30}(001)$ lattice is rotated around the film normal by 45° with respect to the MgO(001) lattice, as shown in Fig. 3. In this configuration, the mismatch between $\text{bcc}\text{-Fe}_{70}\text{Co}_{30}(001)$ crystal and MgO(001)

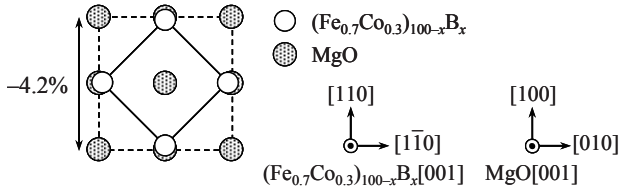


Fig. 3 Planer view schematic diagram of epitaxial orientation relationship of bcc-(Fe_{0.7}Co_{0.3})_{100-x}B_x crystal lattice on MgO(001) substrate.

substrate is calculated by using the lattice constants of bulk Fe₇₀Co₃₀ ($a_{\text{Fe}_{70}\text{Co}_{30}} = 0.2858 \text{ nm}^{17}$) and MgO ($a_{\text{MgO}} = 0.4217 \text{ nm}^{18}$) crystals to be

$$[(\sqrt{2}a_{\text{Fe}_{70}\text{Co}_{30}} - a_{\text{MgO}}) / a_{\text{MgO}}] \times 100 = -4.2\%, \quad (1)$$

which suggests a possibility that the bcc-Fe₇₀Co₃₀ crystal lattice is expanded along the in-plane direction.

The RHEED patterns observed for (Fe_{0.7}Co_{0.3})₉₅B₅ films deposited at 200–600 °C, (Fe_{0.7}Co_{0.3})₉₀B₁₀ films deposited at 400–600 °C, and an (Fe_{0.7}Co_{0.3})₈₅B₁₅ film deposited at 600 °C are respectively shown in Figs. 1(b-2)–(b-4), (c-3)–(c-4), and (d-4). Diffraction patterns from bcc(001) surface are recognized, similar to the case of Fe₇₀Co₃₀ films. (Fe_{0.7}Co_{0.3})_{100-x}B_x single-crystal films of bcc(001) orientation are also obtained for the compositional range of $x = 5$ –15 at. % by using the elevated substrate temperatures.

Figures 1(b-1), (c-2), and (d-3) show the RHEED patterns observed for an (Fe_{0.7}Co_{0.3})₉₅B₅ film deposited at RT, an (Fe_{0.7}Co_{0.3})₉₀B₁₀ film deposited at 200 °C, and an (Fe_{0.7}Co_{0.3})₈₅B₁₅ film deposited at 400 °C, respectively. Diffraction patterns from bcc(122) surface [Fig. 2(b)] are observed in addition to those from bcc(001) surface, as shown in Fig. 2(d). The bcc(122) pattern is analyzed to be an overlap of reflections from two variants, as shown by the indices with subscripts, B and C. The crystallographic orientation relationships are determined as

$$\text{bcc}-(\text{Fe}_{0.7}\text{Co}_{0.3})_{100-x}\text{B}_x(122)[01\bar{1}] \parallel \text{MgO}(001)[100], \quad (\text{type B})$$

$$\text{bcc}-(\text{Fe}_{0.7}\text{Co}_{0.3})_{100-x}\text{B}_x(122)[0\bar{1}1] \parallel \text{MgO}(001)[100]. \quad (\text{type C})$$

When the atomic arrangements of MgO(001) and Fe-Co-B(122) surfaces, which are with four- and one-fold symmetries, are considered, bcc(122) variants with the orientation relationships of

$$\text{bcc}-(\text{Fe}_{0.7}\text{Co}_{0.3})_{100-x}\text{B}_x(122)[4\bar{1}\bar{1}] \parallel \text{MgO}(001)[100], \quad (\text{type D})$$

$$\text{bcc}-(\text{Fe}_{0.7}\text{Co}_{0.3})_{100-x}\text{B}_x(122)[\bar{4}11] \parallel \text{MgO}(001)[100], \quad (\text{type E})$$

are interpreted to be formed. Figure 2(c) shows the schematic diagram of RHEED pattern simulated for the two bcc(122) variants. When the incident electron beam is parallel to MgO[100] (\parallel bcc[4 $\bar{1}\bar{1}$] and bcc[$\bar{4}11$]), there

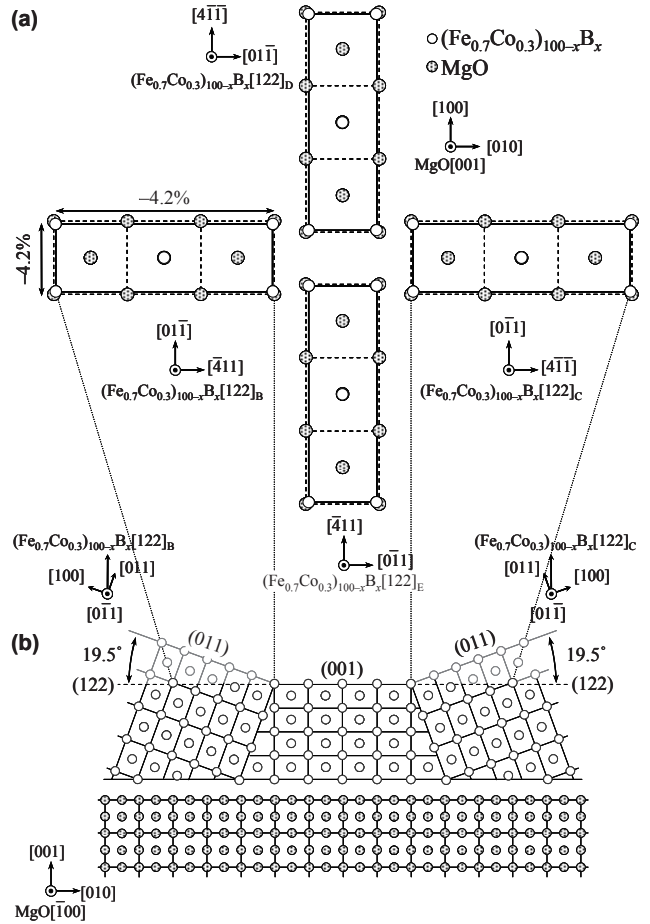


Fig. 4 (a) Planer and (b) cross-sectional view schematic diagrams of epitaxial orientation relationships of bcc-(Fe_{0.7}Co_{0.3})_{100-x}B_x(001) crystal and four bcc-(Fe_{0.7}Co_{0.3})_{100-x}B_x(122) variants on MgO(001) substrate.

are no reflections in the diffraction pattern. Therefore, the Fe-Co-B films are considered to be consisting of bcc(001) crystal and four bcc(122) variants. The structure is similar to the cases of Fe/GaAs(001)¹⁹ and Fe₅₀Co₅₀/SrTiO₃(001)²⁰ systems. Figure 4 shows the planer and cross-sectional view schematic diagrams of orientation relationships of bcc(001) crystal and four bcc(122) variants. The orientations of bcc(122) variants are rotated around the film normal by 90° each other. The lattice misfit values along bcc[01 $\bar{1}$] and bcc[4 $\bar{1}\bar{1}$] are respectively calculated to be

$$[(\sqrt{2}a_{\text{Fe}_{70}\text{Co}_{30}} - a_{\text{MgO}}) / a_{\text{MgO}}] \times 100 = -4.2\%, \quad (2)$$

$$[(3\sqrt{2}a_{\text{Fe}_{70}\text{Co}_{30}} - 3a_{\text{MgO}}) / 3a_{\text{MgO}}] \times 100 = -4.2\%. \quad (3)$$

The misfit values do not differ depending on the in-plane direction and are the same with the lattice mismatch at the bcc(001)/MgO(001) interface. In order to confirm the orientation relationships, a pole-figure XRD measurement was carried out. Figure 5(a) shows the pole-figure XRD pattern of the (Fe_{0.7}Co_{0.3})₈₅B₁₅ film deposited at 400 °C measured by fixing the diffraction

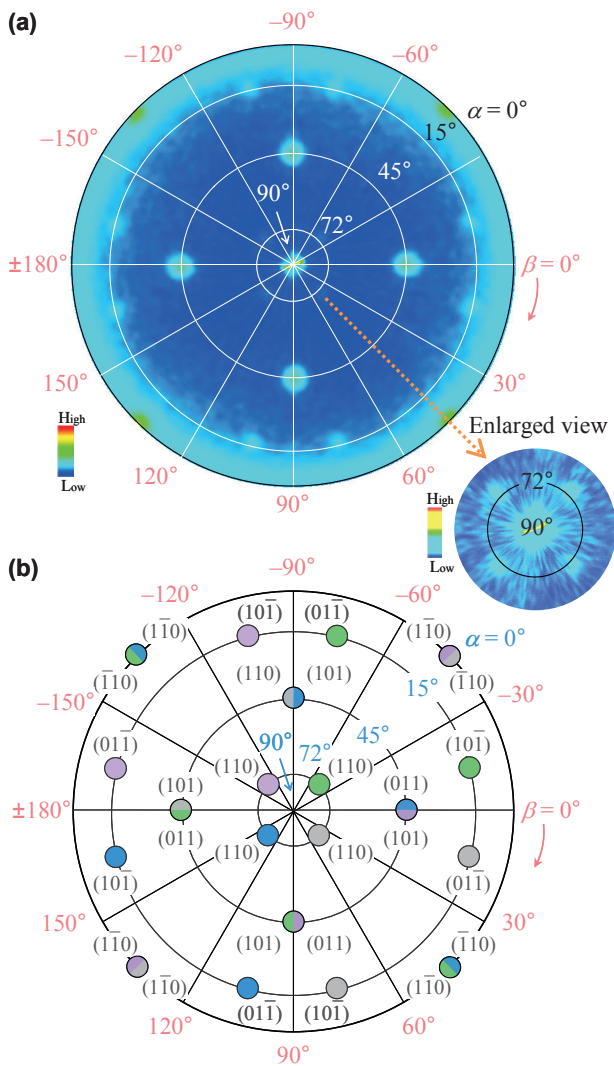


Fig. 5 (a) Pole-figure XRD pattern of $(\text{Fe}_{0.7}\text{Co}_{0.3})_{85}\text{B}_{15}$ film deposited at 400 °C measured by fixing the diffraction angle, $2\theta_B$, at 44.5°. The intensity is shown in logarithmic scale. (b) Schematic diagram obtained by overlapping diffraction patterns simulated for the $\text{bcc}(\text{Fe}_{0.7}\text{Co}_{0.3})_{100-x}\text{B}_x(122)$ variants grown in the orientation relationships determined by RHEED.

angle, $2\theta_B$, at 44.5°, where $\text{bcc}\{110\}$ reflections are expected to be detectable. Figure 5(b) shows the schematic diagram of pole-figure pattern calculated for the four $\text{bcc}(122)$ variants. The experimental pole-figure pattern is in agreement with the simulated result. The pole-figure XRD confirms the crystallographic orientation relationships determined by RHEED.

Figure 1(c-1) shows the RHEED pattern observed for an $(\text{Fe}_{0.7}\text{Co}_{0.3})_{90}\text{B}_{10}$ film deposited at RT. A ring-like diffraction pattern is observed. A polycrystalline $(\text{Fe}_{0.7}\text{Co}_{0.3})_{90}\text{B}_{10}$ film is formed. Figures 1(d-1) and (d-2) show the RHEED patterns observed for $(\text{Fe}_{0.7}\text{Co}_{0.3})_{85}\text{B}_{15}$ films deposited at RT and 200 °C, respectively. Halo diffraction patterns are recognized. Amorphous $(\text{Fe}_{0.7}\text{Co}_{0.3})_{85}\text{B}_{15}$ films are formed.

Figure 6 summarizes the structure and

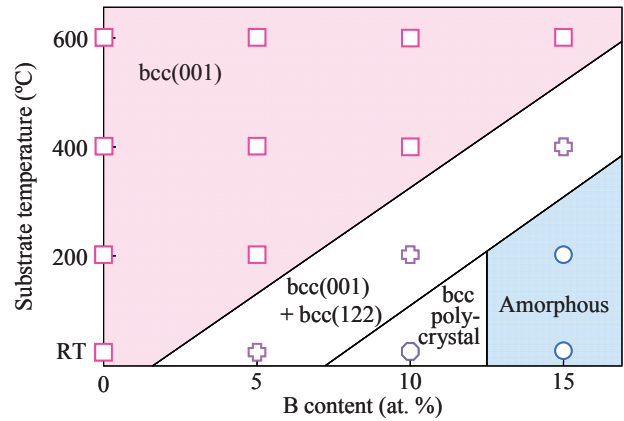


Fig. 6 Phase diagram of $(\text{Fe}_{0.7}\text{Co}_{0.3})_{100-x}\text{B}_x$ film deposited on $\text{MgO}(001)$ substrate.

crystallographic orientation of $(\text{Fe}_{0.7}\text{Co}_{0.3})_{100-x}\text{B}_x$ film deposited on $\text{MgO}(001)$ substrate. The structure varies in the order from $\text{bcc}(001)$ single-crystal, $\text{bcc}(001)$ and $\text{bcc}(122)$ crystals, bcc polycrystal, and to amorphous with increasing the B content and with decreasing the substrate temperature.

3.2 Lattice strain

Figure 7 shows the out-of-plane and in-plane XRD patterns measured for the $(\text{Fe}_{0.7}\text{Co}_{0.3})_{100-x}\text{B}_x$ films with different B contents deposited at 200 °C. Here, the scattering vector of in-plane XRD is parallel to $\text{MgO}[1\bar{1}0]$. As shown in the data of Fig. 6, these four films are consisting of $\text{bcc}(001)$ single-crystals (B content: 0, 5 at. %), mixture of $\text{bcc}(001)$ and $\text{bcc}(122)$ crystals (B content: 10 at. %), and amorphous (B content: 15 at. %), respectively. Strong out-of-plane $\text{bcc}(002)$ and in-plane $\text{bcc}(200)$ reflections are observed for the single-crystal $\text{Fe}_{70}\text{Co}_{30}$ and $(\text{Fe}_{0.7}\text{Co}_{0.3})_{95}\text{B}_5$ films [Figs. 7(a), (b)]. In the XRD patterns measured for the $(\text{Fe}_{0.7}\text{Co}_{0.3})_{90}\text{B}_{10}$ film consisting of $\text{bcc}(001)$ and $\text{bcc}(122)$ variants [Fig. 7(c)], weak out-of-plane and in-plane reflections from $\text{bcc}(001)$ variant are recognized, while reflections from $\text{bcc}(122)$ variants are absent, since the $\text{bcc}(122)$ reflection is forbidden. The present study shows that a combination of RHEED or pole-figure XRD with conventional out-of-plane and in-plane XRDs is effective to determine whether an Fe-Co-B film involves $\text{bcc}(122)$ crystals in addition to $\text{bcc}(001)$ crystal. No reflections from bcc crystals are observed in the out-of-plane and in-plane patterns measured for the amorphous $(\text{Fe}_{0.7}\text{Co}_{0.3})_{85}\text{B}_{15}$ film [Fig. 7(d)].

Figure 8 shows the out-of-plane and in-plane orientation dispersions, $\Delta\theta_{50}$ and $\Delta\theta_{\chi_{50}}$, measured for single-crystal $(\text{Fe}_{0.7}\text{Co}_{0.3})_{100-x}\text{B}_x$ films. Here, the $\Delta\theta_{50}$ and $\Delta\theta_{\chi_{50}}$ values are respectively the full widths at half maximum of ω and φ -scan rocking curves measured by setting the diffraction angles of 2θ and $2\theta_{\chi}$ at the peak angles of $\text{bcc}(002)$ and $\text{bcc}(200)$ reflections. The $\Delta\theta_{50}$ and $\Delta\theta_{\chi_{50}}$ values decrease not only with increasing the

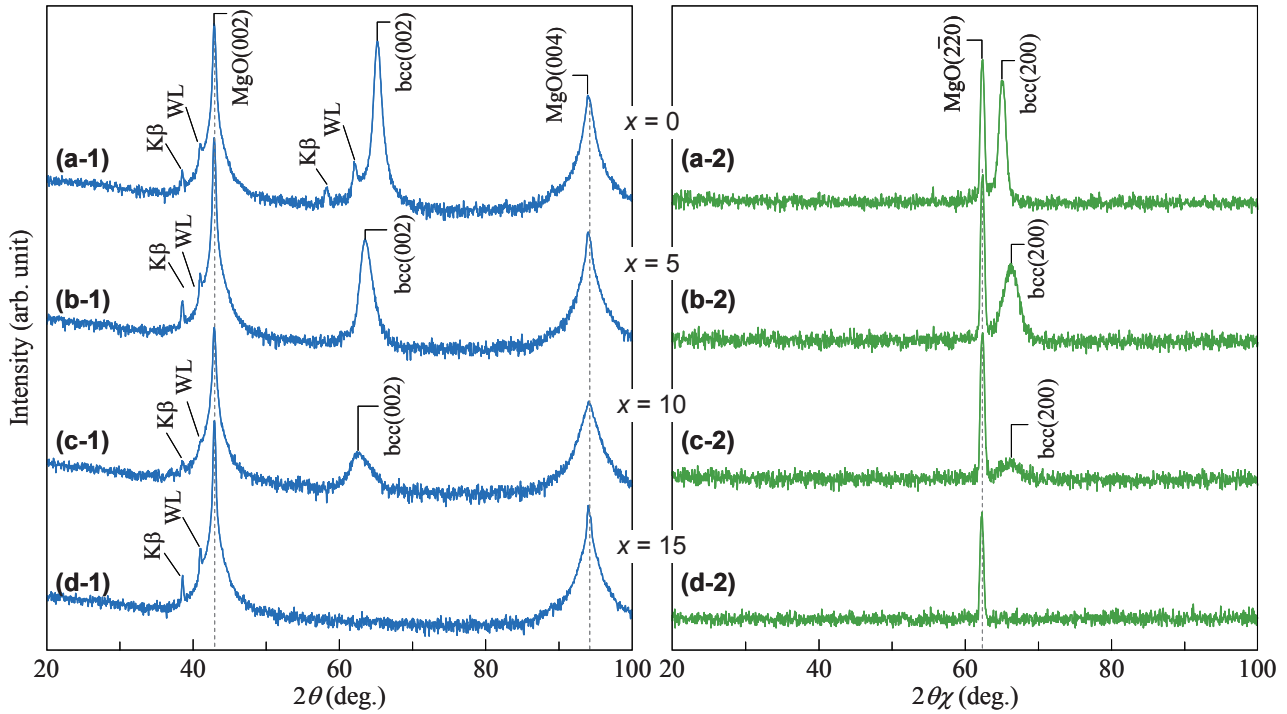


Fig. 7 (a-1)–(d-1) Out-of-plane and (a-2)–(d-2) in-plane XRD patterns measured for $(\text{Fe}_{0.7}\text{Co}_{0.3})_{100-x}\text{B}_x$ films with the B contents of (a) 0, (b) 5, (c) 10, and (d) 15 at. % deposited on MgO(001) substrates at 200 °C. The in-plane XRD patterns are measured by making the scattering vector parallel to MgO[1 $\bar{1}$ 0]. The intensity is shown in logarithmic scale.

substrate temperature but also with decreasing the B content. The crystallographic quality is improved for an $(\text{Fe}_{0.7}\text{Co}_{0.3})_{100-x}\text{B}_x$ film with a lower B content deposited at a higher substrate temperature. The result seems to be related with the structural variation of bcc(001) single-crystal \Rightarrow bcc(001) and bcc(122) crystals \Rightarrow bcc polycrystal \Rightarrow amorphous.

Figure 9 shows the substrate temperature dependences of in-plane and out-of-plane lattice parameters, a and c , and the ratio, d/a , of single-crystal $\text{Fe}_{70}\text{Co}_{30}$ film. Here, the a and the c values are respectively calculated from the peak angles of bcc(002) and bcc(200) reflections by using the relations of

$$a = 2[\lambda / 2\sin(\theta_{\chi})_{\text{bcc}(200)}], \quad (4)$$

$$c = 2[\lambda / 2\sin(\theta)_{\text{bcc}(002)}]. \quad (5)$$

The errors are estimated by using the relationships of

$$(\Delta a) / 2 = \pm \{a [\cot(\theta_{\chi})_{\text{bcc}(200)}] \Delta(\theta_{\chi})_{\text{bcc}(200)}\} / 2, \quad (6)$$

$$(\Delta c) / 2 = \pm \{c [\cot(\theta)_{\text{bcc}(002)}] \Delta(\theta)_{\text{bcc}(002)}\} / 2. \quad (7)$$

For the film deposited at RT, the a value (0.2896 nm) is larger than the c value (0.2836 nm). The in-plane and out-of-plane lattices are respectively expanded and contracted in accommodation of the lattice mismatch of -4.2% existing at the $\text{Fe}_{70}\text{Co}_{30}/\text{MgO}$ interface. With increasing the substrate temperature from RT to 200 °C, the d/a value is approaching to 1. For the substrate temperature range of 200–600 °C, the d/a value is almost kept constant at 1. The lattice deformation is

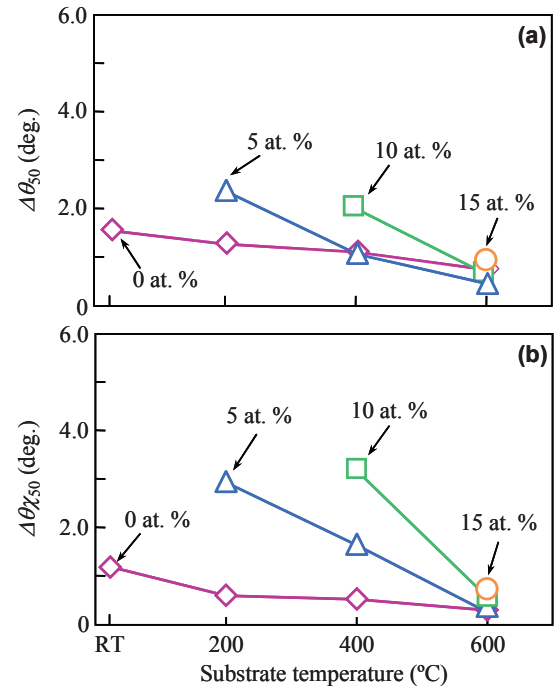


Fig. 8 Substrate temperature dependences of (a) $\Delta\theta_{50}$ and (b) $\Delta\theta_{\chi_{50}}$ values measured for single-crystal $(\text{Fe}_{0.7}\text{Co}_{0.3})_{100-x}\text{B}_x$ films with different B contents.

relaxed by using temperatures higher than 200 °C.

Figure 10 shows the lattice parameters of single-crystal $(\text{Fe}_{0.7}\text{Co}_{0.3})_{100-x}\text{B}_x$ ($x = 5\text{--}15$ at. %) films.

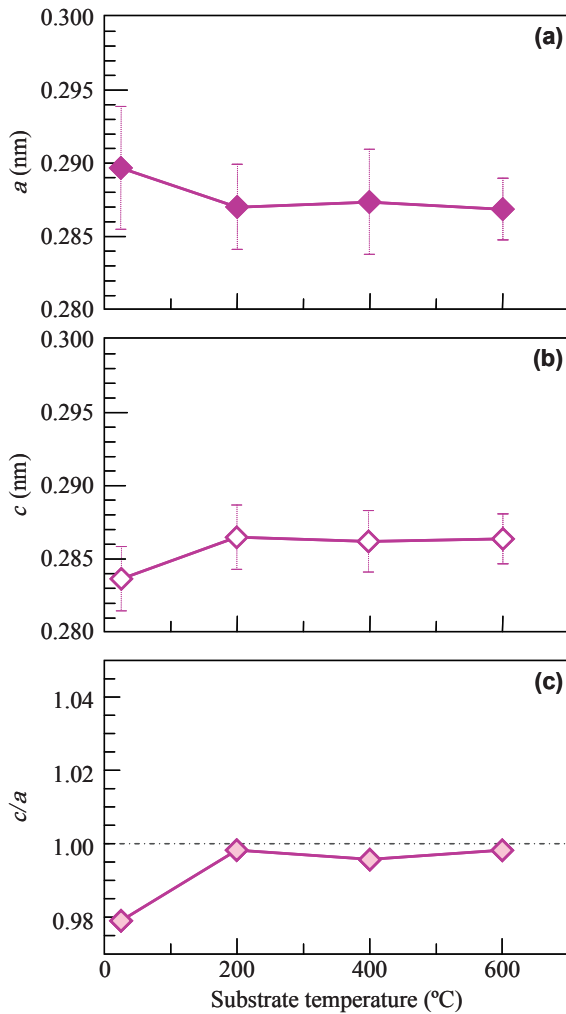


Fig. 9 Lattice parameters, (a) a , (b) c , and (c) d/a , measured for single-crystal $\text{Fe}_{70}\text{Co}_{30}$ films.

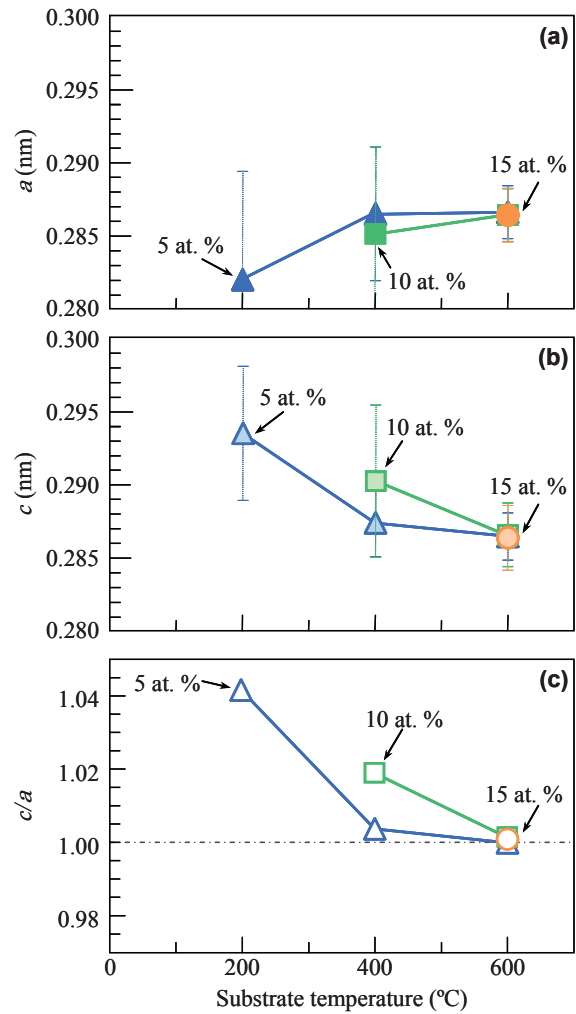


Fig. 10 Lattice parameters, (a) a , (b) c , and (c) d/a , measured for single-crystal $(\text{Fe}_{0.7}\text{Co}_{0.3})_{100-x}\text{B}_x$ ($x = 5-15$ at. %) films.

For the $(\text{Fe}_{0.7}\text{Co}_{0.3})_{95}\text{B}_5$ film deposited at 200 °C, the a value (0.2818 nm) is smaller than the c value (0.2935 nm). The in-plane and out-of-plane lattices are respectively contracted and expanded, though there exists the mismatch with minus sign at the film/substrate interface. The crystal lattice is deformed along the perpendicular direction by addition of B atoms. With increasing the substrate temperature from 200 to 600 °C, the d/a value of $(\text{Fe}_{0.7}\text{Co}_{0.3})_{95}\text{B}_5$ film decreases from 1.042 to 1.000. The lattice strain decreases with increasing the substrate temperature, similar to the case of $\text{Fe}_{70}\text{Co}_{30}$ film. The d/a value (1.019) of $(\text{Fe}_{0.7}\text{Co}_{0.3})_{90}\text{B}_{10}$ film deposited at 400 °C is larger than that (1.004) of $(\text{Fe}_{0.7}\text{Co}_{0.3})_{95}\text{B}_5$ film deposited at 400 °C. A higher B content is apparently enhancing the lattice deformation.

3.3 Surface morphology and magnetic properties

Figure 11 shows the AFM image observed for $\text{Fe}_{70}\text{Co}_{30}$ films deposited at 200–600 °C. The film growth on MgO substrate seems to follow Volmer-Weber²¹⁾ (island-like growth) mode. The film deposited at 200 °C

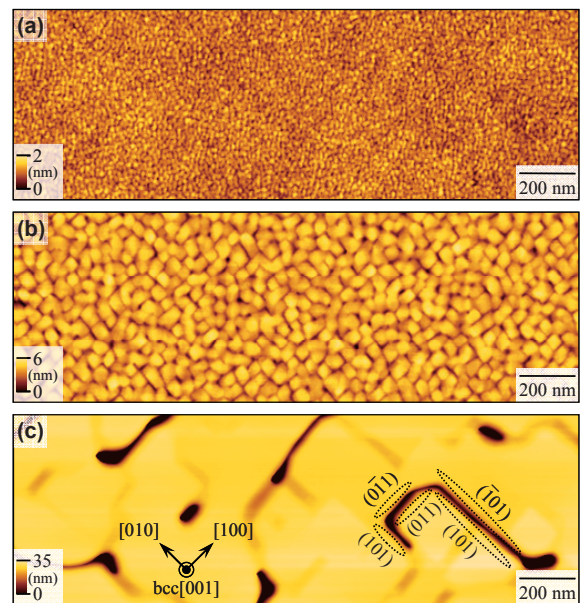


Fig. 11 AFM images observed for $\text{Fe}_{70}\text{Co}_{30}$ films deposited on MgO(001) substrates at (a) 200, (b) 400, and (c) 600 °C.

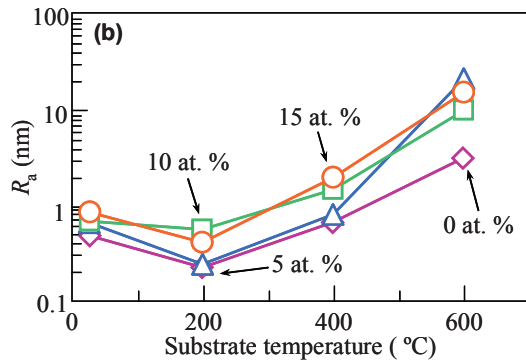


Fig. 12 Substrate temperature dependences of R_a values measured for $(\text{Fe}_{0.7}\text{Co}_{0.3})_{100-x}\text{B}_x$ films with different B contents.

has a flat surface with the arithmetical mean roughness, R_a , of 0.2 nm [Fig. 11(a)]. When the substrate temperature is increased up to 400 °C, an island-like surface involving side $\text{bcc}\{110\}$ facets is recognized [Fig. 11(b)]. The orientations of facets were estimated from

the cross-sectional profiles of the AFM images (not shown here). With further increasing the substrate temperature to 600 °C, the island size drastically increases [Fig. 11(c)]. Migration and clustering of deposited atoms are promoted by employing a higher substrate temperature. Figure 12 summarizes the substrate temperature dependences of R_a values measured for $(\text{Fe}_{0.7}\text{Co}_{0.3})_{100-x}\text{B}_x$ films. Similar tendencies are observed, even though the B contents are different.

Figure 13 shows the in-plane magnetization curves of single-crystal $\text{Fe}_{70}\text{Co}_{30}$ films deposited at different temperatures measured by applying the magnetic field along $\text{bcc}[100]$ or $\text{bcc}[110]$. The films are easily magnetized when the magnetic field is applied along $\text{bcc}[100]$, while the magnetization curves measured along $\text{bcc}[110]$ saturate at higher magnetic fields. There were no clear differences in the hysteresis loops measured along $\text{bcc}[100]$ and $\text{bcc}[010]$ and measured along $\text{bcc}[110]$ and $\text{bcc}[1\bar{1}0]$ (not shown here). Therefore, the films show four-fold symmetries in in-plane magnetic anisotropies, which are reflecting the

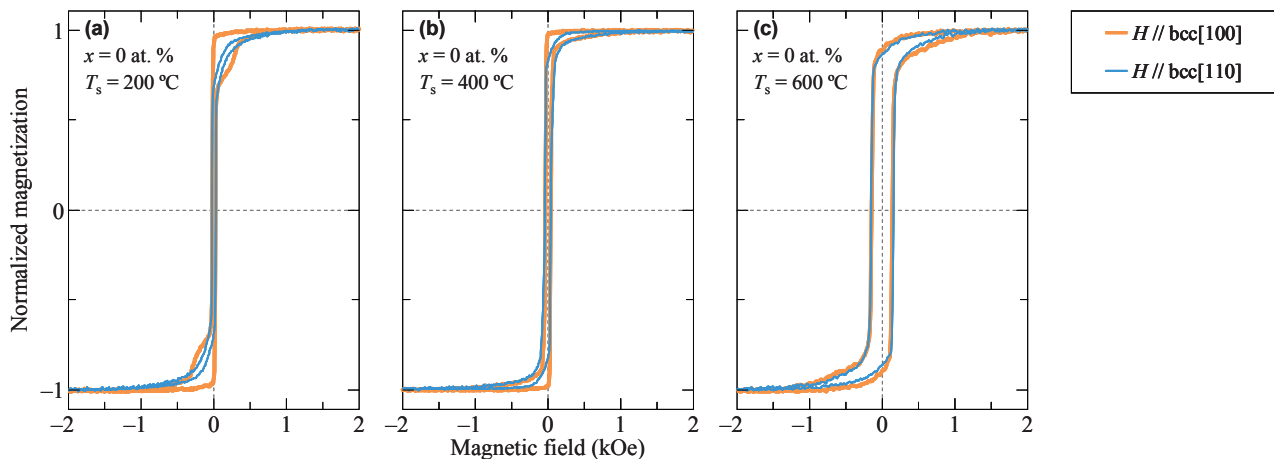


Fig. 13 In-plane magnetization curves measured for single-crystal $\text{Fe}_{70}\text{Co}_{30}$ films formed at (a) 200, (b) 400, and (c) 600 °C. The magnetic field is applied along $\text{bcc}[100]$ or $\text{bcc}[110]$.

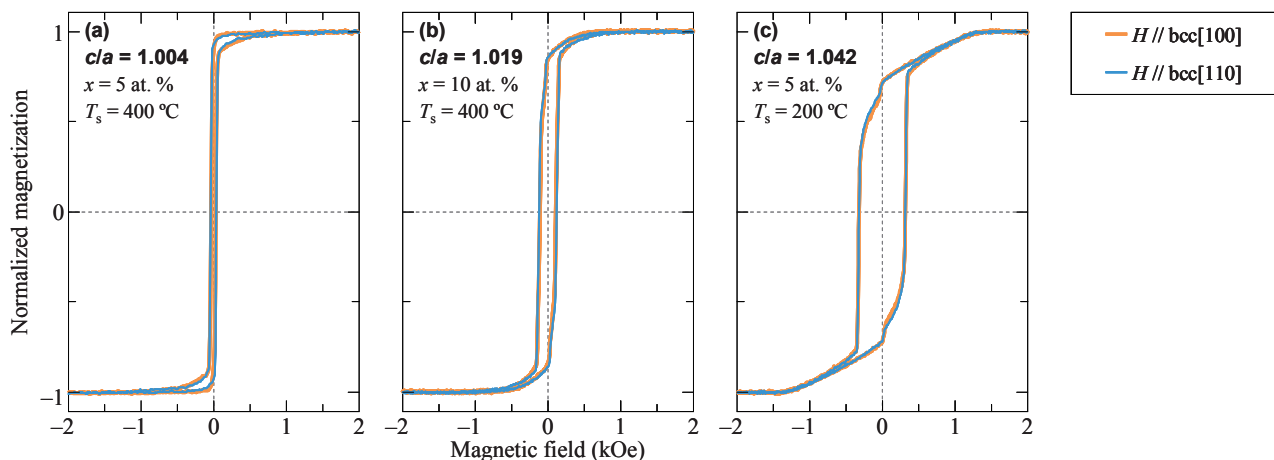


Fig. 14 In-plane magnetization curves measured for single-crystal $(\text{Fe}_{0.7}\text{Co}_{0.3})_{100-x}\text{B}_x$ films with the c/a ratios of (a) 1.004, (b) 1.019, (c) 1.042. The magnetic field is applied along $\text{bcc}[100]$ or $\text{bcc}[110]$.

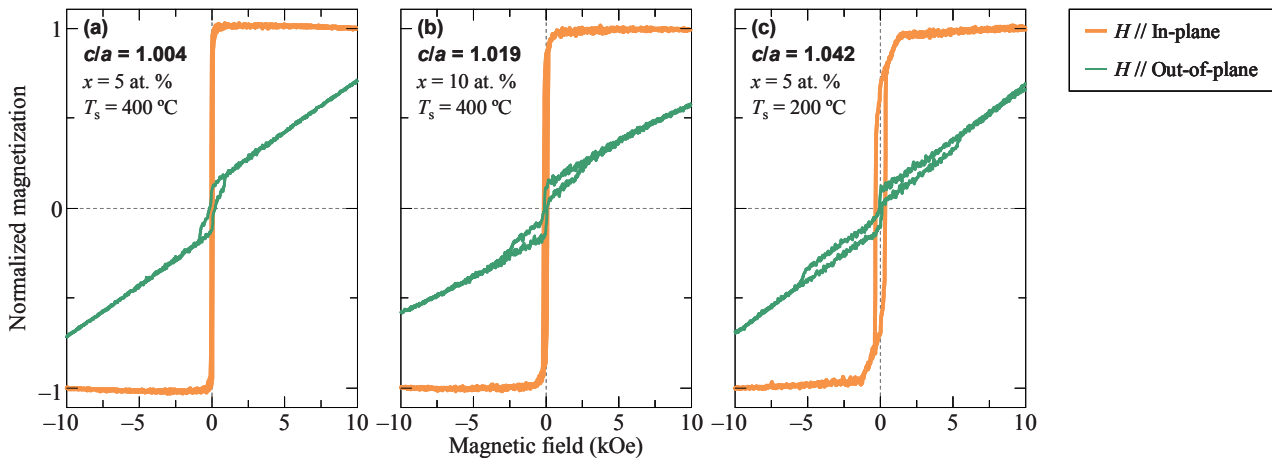


Fig. 15 Out-of-plane and in-plane magnetization curves measured for single-crystal $(\text{Fe}_{0.7}\text{Co}_{0.3})_{100-x}\text{B}_x$ films with the c/a ratios of (a) 1.004, (b) 1.019, and (c) 1.042.

magnetocrystalline anisotropy of bulk $\text{Fe}_{70}\text{Co}_{30}$ alloy with the easy magnetization axes of $\text{bcc}\langle 100 \rangle$. The in-plane anisotropy decreases as the substrate temperature increases. The magnetic anisotropy seems to be influenced not only by the magnetocrystalline anisotropy but also by the shape anisotropy caused by the surface undulation, which is more enhanced by using a higher substrate temperature. With increasing the substrate temperature from 200 to 600 °C, the coercivity of hysteresis curve measured along $\text{bcc}[100]$ increases from 2.5 to 150 Oe. Domain wall motion seems to be suppressed by the crevasses existing between islands, as shown in the AFM image of Fig. 11(c).

Figure 14 shows the in-plane magnetization curves of single-crystal $(\text{Fe}_{0.7}\text{Co}_{0.3})_{100-x}\text{B}_x$ films with the c/a ratios of 1.004, 1.019, and 1.042 whose B contents are 5, 10, and 5 at. % and whose formation temperatures are 400, 400, and 200 °C, respectively. Although the films are composed of $\text{bcc}(001)$ single-crystal, almost isotropic in-plane curves are observed. As the c/a ratio increases from 1.004 to 1.042, the coercivity increases from 30 to 320 Oe, whereas the remnant magnetization, M_r/M_s , decreases from 0.923 to 0.718. The result indicates that perpendicular magnetic anisotropies have been also induced in the strained $(\text{Fe}_{0.7}\text{Co}_{0.3})_{100-x}\text{B}_x$ single-crystal films, similar to the cases of previous studies^{9–16}. Figure 15 shows the out-of-plane and in-plane hysteresis loops measured for the $(\text{Fe}_{0.7}\text{Co}_{0.3})_{100-x}\text{B}_x$ films. The films show weak perpendicular magnetic anisotropies. The perpendicular magnetic anisotropy seems to have been slightly enhanced with increasing the c/a ratio. The magnetic properties are apparently influenced by the lattice deformation.

4. Conclusion

$(\text{Fe}_{0.7}\text{Co}_{0.3})_{100-x}\text{B}_x$ alloy films are prepared by sputter deposition on $\text{MgO}(001)$ substrates by varying the B content from 0 to 15 at. % and by varying the substrate temperature from RT to 600 °C. The detailed

structural properties are investigated by RHEED and XRD. Single-crystal $(\text{Fe}_{0.7}\text{Co}_{0.3})_{100-x}\text{B}_x$ films with the B contents of 0, 5, 10, and 15 at. % are formed at temperatures higher than RT, 200 °C, 400 °C, and 600 °C, respectively. The crystallographic orientation relationship is $\text{bcc}-(\text{Fe}_{0.7}\text{Co}_{0.3})_{100-x}\text{B}_x(001)[110] \parallel \text{MgO}(001)[100]$. As the B content increases and the substrate temperature decreases, the structure varies in the order of $\text{bcc}(001)$ single-crystal \Rightarrow a mixture of $\text{bcc}(001)$ and $\text{bcc}(122)$ crystals \Rightarrow polycrystal \Rightarrow amorphous. The lattice of single-crystal $\text{Fe}_{70}\text{Co}_{30}$ film is expanded along the in-plane direction in accommodation of the mismatch existing at the $\text{Fe}_{70}\text{Co}_{30}(001)/\text{MgO}(001)$ interface. On the contrary, the lattices of single-crystal $(\text{Fe}_{0.7}\text{Co}_{0.3})_{100-x}\text{B}_x$ ($x = 5\text{--}15$ at. %) films are expanded along the perpendicular direction. The $\text{Fe}_{70}\text{Co}_{30}$ films show in-plane magnetic anisotropies reflecting the magnetocrystalline anisotropy of bulk $\text{Fe}_{70}\text{Co}_{30}$ crystal, whereas the $(\text{Fe}_{0.7}\text{Co}_{0.3})_{100-x}\text{B}_x$ films show weak perpendicular magnetic anisotropies, which are possibly caused by an influence of lattice strain along the perpendicular direction.

Acknowledgement A part of this work was supported by Chuo University Grant for Special Research.

References

- 1) S. S. P. Parkin, C. Kaiser, A. Panchula, P. M. Rice, B. Hughes, M. Samant, and S. H. Yang: *Nature Mater.*, **3**, 862 (2004).
- 2) S. Yuasa, T. Nagahama, A. Fukushima, Y. Suzuki, and K. Ando: *Nature Mater.*, **3**, 868 (2004).
- 3) Y. Asai, M. Ohtake, T. Kawai, and M. Futamoto: *J. Korean Phys. Soc.*, **63** 733 (2013).
- 4) L. Reichel, L. Schultz, D. Pohl, S. Oswald, S. Fähler, M. Werwiński, A. Edström, E. K. Delczeg-Czirjak, and J. Rusz: *J. Phys.: Condens. Matter*, **27** 476002 (2015).
- 5) Y. H. Ghang, S. W. Yung, T. S. Chin, and M. P. Hung: *Jpn. J. Appl. Phys.*, **26**, 2041 (1987).
- 6) J. Yu, C. Chang, D. Karns, G. Ju, Y. Kubota, W. Eppler, C.

- Brucker, and D. Weller: *J. Appl. Phys.*, **91**, 8357 (2002).
- 7) K. Lee, J. J. Sapan, S. H. Kang, and E. E. Fullerton: *J. Appl. Phys.*, **109**, 123910 (2011).
 - 8) N. Sato, R. M. White, and S. X. Wang: *J. Appl. Phys.*, **108**, 152405 (2016).
 - 9) W. B. Person: *A Handbook of Lattice Spacings and Structures of Metals and Alloys* (Pergamon Press, London, New York, Los Angeles, Paris, 1958) pp. 504–505.
 - 10) J. Yamashita and S. Asano: *J. Phys. Soc. Jpn.*, **52**, 3506 (1983).
 - 11) K. Matsubara, M. Ohtake, K. Tobari, and M. Futamoto: *Thin Solid Films*, **519**, 8299 (2011).
 - 12) T. Nishiyama, K. Shikada, M. Ohtake, F. Kirino, and M. Futamoto: *J. Magn. Soc. Jpn.*, **34**, 5 (2010).
 - 13) J. A. Venable: *Introduction to Surface and Thin Film Process* (Cambridge Univ. Press, New York, 2000) pp. 145–147.
 - 14) T. Burkert, L. Nordström, O. Eriksson, and O. Heinonen: *Phys. Rev. Lett.*, **93**, 027203 (2004).
 - 15) Y. Kota and A. Sakuma: *J. Magn. Soc. Jpn.*, **37**, 17 (2013).
 - 16) G. Andersson, T. Burkert, P. Warnicke, M. Björck, B. Sanyal, C. Chacon, C. Zlotea, L. Nordström, P. Nordblad, and O. Eriksson: *Phys. Rev. Lett.*, **96**, 037205 (2006).
 - 17) A. Winkelmann, M. Przybylski, F. Luo, Y. Shi, and J. Barthel: *Phys. Rev. Lett.*, **96**, 257205 (2006).
 - 18) F. Yildiz, M. Przybylski, X. -D. Ma, and J. Kirschner: *Phys. Rev. B*, **80**, 064415 (2009).
 - 19) B. Lao, J. W. Jung, and M. Sahashi: *IEEE Trans. Magn.*, **50**, 2008704 (2014).
 - 20) H. Oomiya, B. Wang, S. Yoshida, T. Kataguchi, K. Takahashi, S. Kanatani, L. Zhang, L. Liu, T. Hasegawa, K. Hayasaka, S. Saito, N. Inami, T. Ueno, K. Ono, and S. Ishio: *J. Phys. D: Appl. Phys.*, **48**, 475003 (2015).
 - 21) S. Ishio, T. Hasegawa, S. Yoshida, S. Kanatani, K. Takahashi, K. Kumagaya, and M. Hirao: *Magnetics Jpn.*, **12**, 21 (2017).

Received Apr. 4, 2017; Accepted Jun. 10, 2017